Available online at www.sciencedirect.com

ScienceDirect

Trans. Nonferrous Met. Soc. China 34(2024) 2507−2520

Transactions of
Nonferrous Metals
Society of China

www.tnmsc.cn

Structural, mechanical and electronic properties of precipitates in Mg−Zn alloys

Tian-zhi ZHANG[1], Yang-zhen LIU[1,2], Qing-yun FU[3], Bai-song GUO[1], Wei-hong JIN[1], Zhen-tao YU[1]

1. Institute of Advance Wear & Corrosion Resistant and Functional Materials,
Jinan University, Guangzhou 510632, China;
2. Shaoguan Research Institute of Jinan University, Shaoguan 512027, China;
3. Stomatological Hospital, Southern Medical University, Guangzhou 510280, China

Received 1 February 2023; accepted 4 July 2023

Abstract: To accelerate the development and design of magnesium (Mg) alloys, the structural and mechanical properties of important precipitates in Mg−Zn alloys were studied by experiments and density functional theory. The nano-indentation tests revealed that the hardness of the precipitates initially increased and then decreased with increasing Zn content, and was significantly higher than that of pure Mg and Zn. The calculation results revealed that the precipitates stability initially increased and then decreased with increasing Zn concentration. The bulk moduli of the precipitates increased, whereas their shear and Young's moduli initially increased and then decreased with increasing Zn content. The decreasing order of ductility for these compounds is $MgZn_2 > Mg_{21}Zn_{25} > Mg_2Zn_{11} > Mg_4Zn_7$. The surface profiles of the compounds revealed that they are obvious anisotropy. Both the degree of covalency and bond length of covalent bonds initially increased and then decreased with increasing Zn content.

Key words: Mg−Zn alloy; nano-indentation; modulus; hardness; chemical bonding

1 Introduction

As one of the lightest materials available (low density of 1.74−2.0 g/cm^3), magnesium (Mg) is widely used in aerospace, automotive and consumer electronics products [1−3]. With the improvement of people's living standards, the number of patients with various types of cardiovascular disease and osteoarthritis is increasing. Thus, the market demand for biomedical metal materials is developing rapidly. Through researchers' relentless efforts, it has been found that Mg possesses an elastic modulus similar to the human body (41−45 GPa) and good biocompatibility and degradability, which makes it a new generation of biomedical materials that attract attention, and has been applied in cardiovascular stents, bone joints and bone nails [4−6]. However, its poor plastic deformation properties and poor corrosion resistance seriously limit its further application. How to improve the properties of Mg has become one of the most important research topics. Therefore, numerous studies have found that alloying is one of the most effective ways to improve the comprehensive properties of Mg alloys [7−11]. It is found that most Mg alloys are mainly concentrated with Y, La and other heavy rare earth elements. Although their addition can greatly improve the comprehensive properties of Mg alloys, the high cost of these additives further limits their commercial application and promotion.

Corresponding author: Yang-zhen LIU, Tel/Fax: +86-20-85220890, E-mail: yangzhenliu@jnu.edu.cn;
Zhen-tao YU, Tel/Fax: +86-20-85220890, E-mail: ninyzt@163.com

DOI: 10.1016/S1003-6326(24)66556-8

Thus, there is an urgent need to seek a low-cost, high-performance Mg-based alloying element.

As one of the essential trace elements for the human body and owing to its low price, zinc (Zn) has attracted increasing attention from researchers. It has been shown that the addition of a small amount of Zn to Mg can not only increase the strength of the material but also improve its biocompatibility [12−14]. Moreover, the maximum solution solubility of Zn in Mg is 6.2 wt.%, and the strengthening methods are solution strengthening and aging strengthening. Aging strengthening is performed using the precipitation of solid-dissolved alloy elements in the form of the intermetallic compounds after the heat treatment to form dispersively distributed particles and improve the strength of the material. It is well known that the type of precipitates is the main factor that determines the strength of the material; thus, the study of precipitate properties is very important. LIU et al [15] and XIE et al [16] have reported that the main precipitates in Mg−Zn alloys are Mg_2Zn_{11}, Mg_4Zn_7, $MgZn_2$ and $Mg_{21}Zn_{25}$. Although the structure and orientation of the precipitates can be observed by X-ray diffraction and transmission electron microscopy based on numerous experiments, their accuracy is sometimes questioned because experimental observation is usually post hoc rather than real-time monitoring and it is only a local observation of the specimen, which cannot reflect integrity. Recently, with the rapid development of computer technology, first-principles calculation has become an effective method for determining the phase stability and sequence of precipitation. For instance, WANG et al [17] have used first-principles calculation to elucidate the crystal structures and formation energies of a very large set of precipitates in Mg−(Nd, Gd, Y, Y−Nd, Nd−Zn, Al and Sn) alloy systems and revealed that the bulk formation energies per solute atom decreased along the observed sequences of precipitation, validating from experiments. KIM et al [18,19] and MAO et al [20] have studied the crystal structure and stability of precipitates in Al alloys using first-principles calculation. OUYANG et al [21] have theoretically studied the structural and mechanical properties of important precipitates in Al−Cu alloy, which provided effective guidance for understanding the mechanism of precipitate strengthening during heat treatment and aging process. However, the sequence, properties and strengthening mechanism of precipitates in Mg−Zn alloys are still unclear. This has seriously hindered the design and development of low-cost and high-performance Mg alloys. Thus, it is necessary to explore the stability, mechanical and electronic properties of precipitates in Mg−Zn alloys through experimental and theoretical studies.

In this study, Mg−Zn alloys were prepared and the morphology and mechanical properties of precipitates were discussed. Additionally, the structural, stability, mechanical and electronic properties of the main precipitates in the Mg−Zn binary system were estimated by experiments and density functional theory. The results are expected to provide an intensive understanding of the nature of aging precipitation phases in Mg−Zn alloys and provide theoretical and experimental data to support the design of high-performance Mg alloys.

2 Methods and computational details

2.1 Specimen preparation

Mg−Zn alloys were prepared using pure Mg (99.9 wt.%) and Zn (99.9 wt.%) ingots (Dongguan Eontec Co., Ltd.) and melting them at 973−1023 K in an electric resistance furnace of 3.5 kW under an argon protective atmosphere. After mechanical stirring for 20 min and degassing, the alloy melts were poured into a preheated steel mould. The chemical compositions of the Mg−Zn alloys were estimated using inductively coupled plasma-atomic emission spectrometry (ICP-AES, Thermo Icap 7000 SERIES, USA) method (Table 1). The as-cast ingots were placed in the furnace, annealed at 300 °C for 24 h and then quenched in water.

Table 1 Chemical compositions of specimens (wt.%)

Specimen	Zn	Mg
A1	7.78	Bal.
A2	10.52	Bal.

2.2 Materials characterization and tests

The test specimens were cut from the core of the block by electric discharge machining. Afterwards, they were polished and etched with a 4% nitric acid solution. The crystalline phase of the specimens was identified using X-ray diffraction (XRD) using an Ultima IV diffractometer (Rigaku, Tokyo, Japan) with monochromatic Cu K_α radiation. The microstructure was analyzed using field emission scanning electron microscopy (Zeiss Gemini SEM 500) equipped with energy dispersive spectroscopy (EDS). Young's moduli and hardness were evaluated using a nano-indenter (Keysight G200, Agilent Technology, USA) with an in-depth control (2000 nm). The corresponding energy was estimated from the load−displacement curve. Each specimen was tested five times to ensure experimental reliability.

2.3 Computational details

The structural, mechanical and electronic properties of the precipitates in the Mg−Zn binary system were discussed using first-principles calculations based on density functional theory, which were performed in the CASTEP package [22]. Ultrasoft pseudopotential was used to describe the interaction between ionic cores and valence electrons. The valence electrons of Mg and Zn are $2p^6 3s^2$ and $3d^{10}4s^2$. The exchange-correlation energy was estimated using the generalized gradient approximation with Perdew–Burke–Ernzerhof (PBE) functional [23]. The cut-off energy was 500 eV. The Brillouin zone integration was achieved by special *k*-point sampling of the Monkhorst−Pack type. Here, the *k*-point meshes of Mg, Mg_2Zn_{11}, Mg_4Zn_7, $MgZn_2$, $Mg_{21}Zn_{25}$ and Zn were set as 9×9×6, 4×4×4, 2×2×2, 8×8×4, 4×4×4 and 5×2×1, respectively. The crystal structures of the precipitates in the Mg−Zn binary system were optimized using the Broyden−Fletcher−Goldfarb−Shannon algorithm. In this study, the total energy converged to 1.0×10^{-6} eV/atom and the force per atom was reduced to 0.03 eV/Å. The crystal structures of the precipitates in the Mg−Zn binary system are shown in Fig. 1.

2.4 Calculation of stability and mechanical properties

To illustrate the stability of the compound, cohesive energy ($E_{\rm coh}$) and formation enthalpy ($\Delta_{\rm r}H_{\rm m}$) were estimated using the following equations [24]:

$$E_{\rm coh}({\rm Mg}_x{\rm Zn}_y)=\frac{E_{\rm tot}({\rm Mg}_x{\rm Zn}_y)-xE_{\rm iso}({\rm Mg})-yE_{\rm iso}({\rm Zn})}{x+y} \quad (1)$$

$$\Delta_{\rm r}H_{\rm m}({\rm Mg}_x{\rm Zn}_y)=\frac{E_{\rm tot}({\rm Mg}_x{\rm Zn}_y)-xE_{\rm bulk}({\rm Mg})-yE_{\rm bulk}({\rm Zn})}{x+y} \quad (2)$$

where $E_{\rm tot}({\rm Mg}_x{\rm Zn}_y)$ is the total energy of the Mg−Zn intermetallic compound, $E_{\rm iso}$ is the energy of atoms in the free state, $E_{\rm bulk}$ is the chemical potential of atoms in the free state, and x and y are the numbers of atoms of Mg and Zn atoms in the unit cell, respectively.

Elastic constants of the Mg−Zn compounds were calculated using the stress−strain method. Different strains were applied to the compounds, and the corresponding stresses can be obtained based on Hooke's law. Afterwards, the elastic

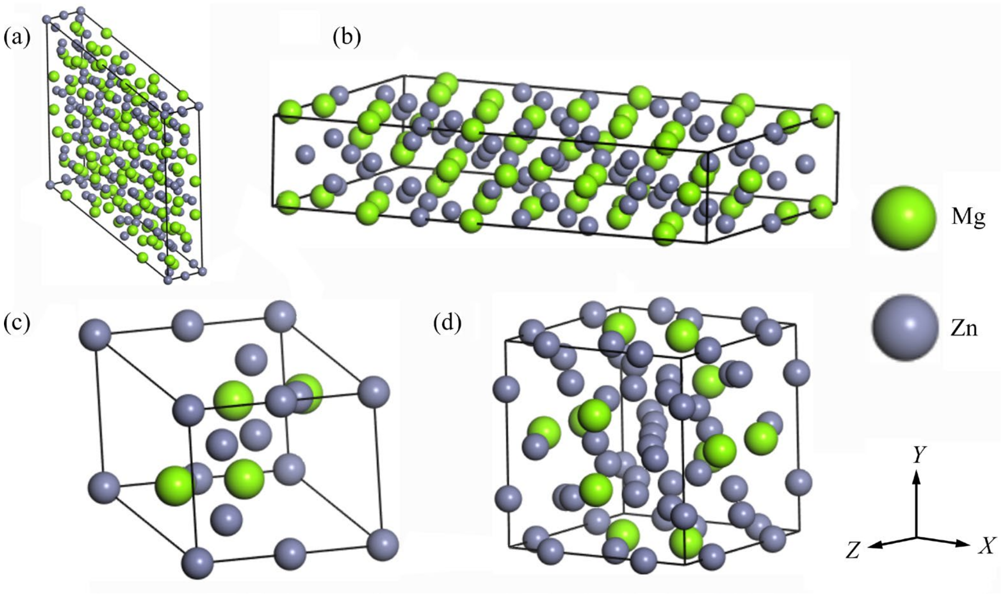

Fig. 1 Crystal structures of precipitates in Mg−Zn alloys: (a) $Mg_{21}Zn_{25}$; (b) Mg_4Zn_7; (c) $MgZn_2$; (d) Mg_2Zn_{11}

constants with different crystal systems can be obtained from the curvature of the energy as a function of strain. Bulk modulus (*B*), shear modulus (*G*), Young's modulus (*E*) and Poisson's ratio (*v*) were estimated from elastic constants using Voigt−Reuss−Hill (VRH) approximation. The calculation expressions are as follows [25]:

$$E=\frac{9B_{\mathrm{VRH}}G_{\mathrm{VRH}}}{3B_{\mathrm{VRH}}+G_{\mathrm{VRH}}} \tag{3}$$

$$v=\frac{3B_{\mathrm{VRH}}-2G_{\mathrm{VRH}}}{2(3B_{\mathrm{VRH}}+G_{\mathrm{VRH}})} \tag{4}$$

where V, R and H refer to the Voigt, Reuss and Hill approximation methods, respectively. They have different calculation methods for different crystal systems. For more details, readers may refer to Refs. [26−28].

3 Results and discussion

3.1 Microstructure of Mg−Zn alloy

To illustrate the phase compositions in the specimens, the XRD patterns of the A1 and A2 specimens are shown in Fig. 2. Pure Mg and pure Zn are used as references to demonstrate the experimental accuracy and reliability. It can be clearly seen in Fig. 2 that the A1 specimen contains Mg_4Zn_7 and $Mg_{21}Zn_{25}$, while the A2 specimen mainly contains $MgZn_2$ and Mg_2Zn_{11}. Similarly, the same phase is observed in similar alloy compositions studied by YAO et al [29]. In the A1 and A2 specimens, the volume fractions of $Mg_{21}Zn_{25}$ and Mg_2Zn_{11} are relatively small. Detailed analysis can be observed by subsequent SEM images. Figure 3 depicts the SEM images of the A1 and A2 alloys accompanied by pure Mg and Zn. As can be seen, eutectic phases have formed mainly along the grain boundaries of Mg after adding Zn. The eutectic phases are mainly Mg−Zn intermetallic compounds. The phase compositions in the A1 and A2 specimens obtained by EDS are listed in Table 2. Based on NEGRI et al [30], the $Mg_{21}Zn_{25}$ intermetallic compound can also be described as equiatomic MgZn while Mg_4Zn_7 can also be represented by Mg_2Zn_3. Based on the EDS results (Table 2) and the previous works [31,32], the precipitates in the A1 specimen are mainly Mg_4Zn_7 and $Mg_{21}Zn_{25}$ while the phase compositions

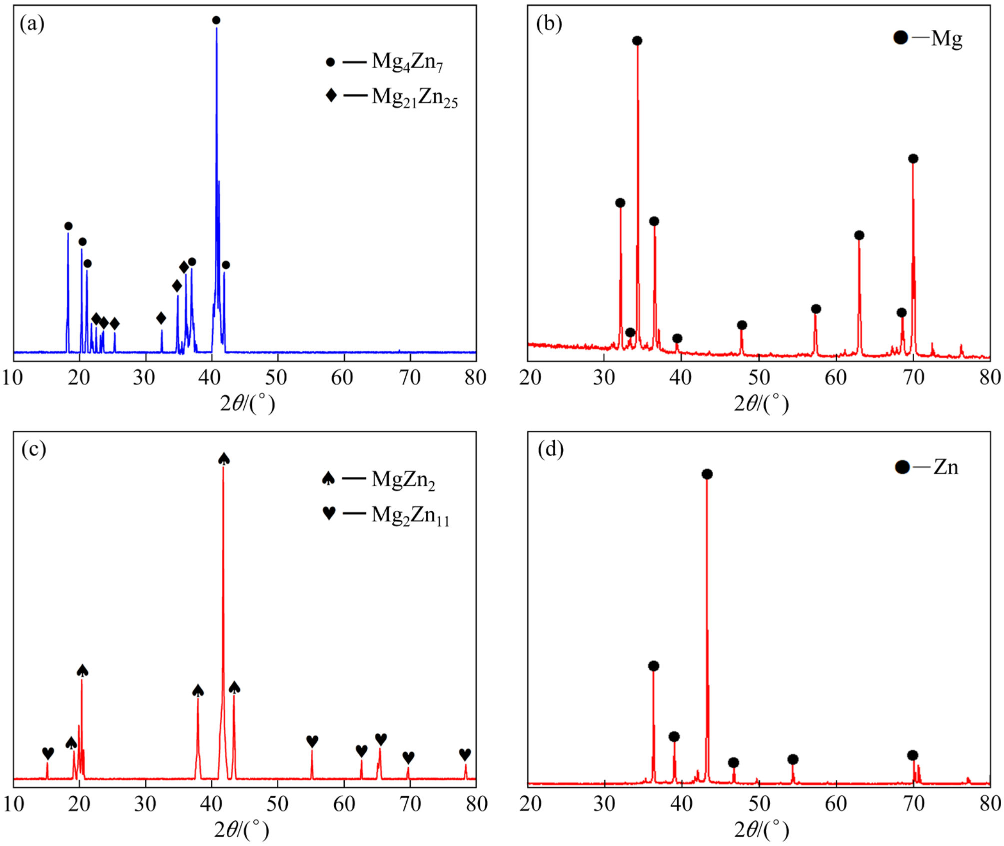

Fig. 2 XRD patterns of specimens: (a) A1; (b) pure Mg; (c) A2; (d) Pure Zn

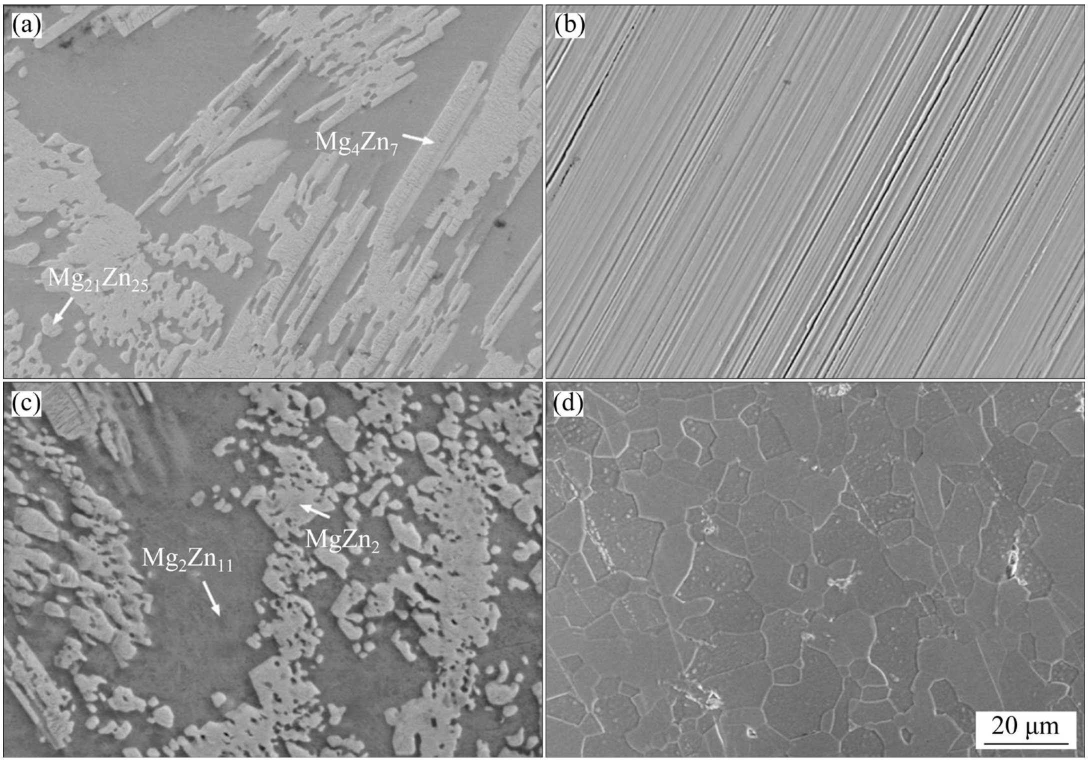

Fig. 3 SEM images of etched specimens with different Zn contents: (a) A1; (b) Pure Mg; (c) A2; (d) Pure Zn

Table 2 Phase compositions in A1 and A2 specimens measured by EDS

Specimen	Phase	Content/at.%	
		Mg	Zn
A1	Mg_4Zn_7	37.20	62.80
	$Mg_{21}Zn_{25}$	49.04	50.96
A2	$MgZn_2$	33.91	66.09
	Mg_2Zn_{11}	16.02	83.98

in the A2 specimen are $MgZn_2$ and Mg_2Zn_{11}, which are consistent with the above XRD results (Fig. 2). Thus, the main precipitates ($Mg_{21}Zn_{25}$, Mg_4Zn_7, $MgZn_2$ and Mg_2Zn_{11}) in the Mg−Zn alloys have been successfully observed experimentally. It is well known that the structure of the precipitates plays a decisive role in alloy properties. Thus, it is very important to understand the properties of precipitates, and the research results provide a theoretical and experimental basis for designing high-performance Mg−Zn alloys.

3.2 Measured mechanical properties of precipitates

The mechanical properties of the precipitated phases in the Mg−Zn alloys are estimated by nano-indentation. Based on the load−displacement curve, the Oliver−Pharr method is used to evaluate the hardness and Young's modulus [33,34]. For the sake of comparison and to illustrate reliability, Young's modulus and hardness of pure Mg and Zn are also given and the detailed Young's modulus and hardness of the precipitates are presented in Table 3. The variation trends of hardness and Young's modulus with Zn content are described in Fig. 4. It can be seen that the measured Young's modulus and hardness of the Mg−Zn binary compounds are in excellent agreement with the results of other studies [35]. The precipitates have significantly higher hardness than pure Mg and Zn. Owing to the high Young's modulus of pure Zn, the increase in Young's modulus for the precipitates is not obvious. Young's modulus and hardness initially increased and then decreased with increasing Zn content. Mg_2Zn_{11} has the highest Young's modulus (92.55 GPa), and Mg_4Zn_7 possesses the highest hardness (5.07 GPa). The evolution of intrinsic Young's modulus and hardness of the precipitates with different Zn contents will be discussed in the next section combined with the calculated elastic properties and electronic structures of the precipitates.

3.3 Structural stability of precipitates

In this section, the optimized lattice parameters and stability of the Mg−Zn compounds are analyzed and the theoretical and experimental results are provided in Table 4. The agreement between our calculated lattice parameters and other available data [31,35−38] is fairly good, with an average error of less than 1%. This slight error may come from experimental conditions or different calculation accuracies. The results indicate that the calculation parameters are set reasonably and our calculated results are acceptable.

To illustrate the stability of the precipitates, cohesive energy and formation enthalpy are calculated using Eqs. (1) and (2), respectively, as listed in Table 4. Cohesive energy is defined as the energy required to decompose the compound into individual atoms and is related to the structural stability of the compound [39]. The smaller the cohesive energy is, the better the structural stability is. Formation enthalpy is the alloying ability of a crystal. A negative formation enthalpy means that

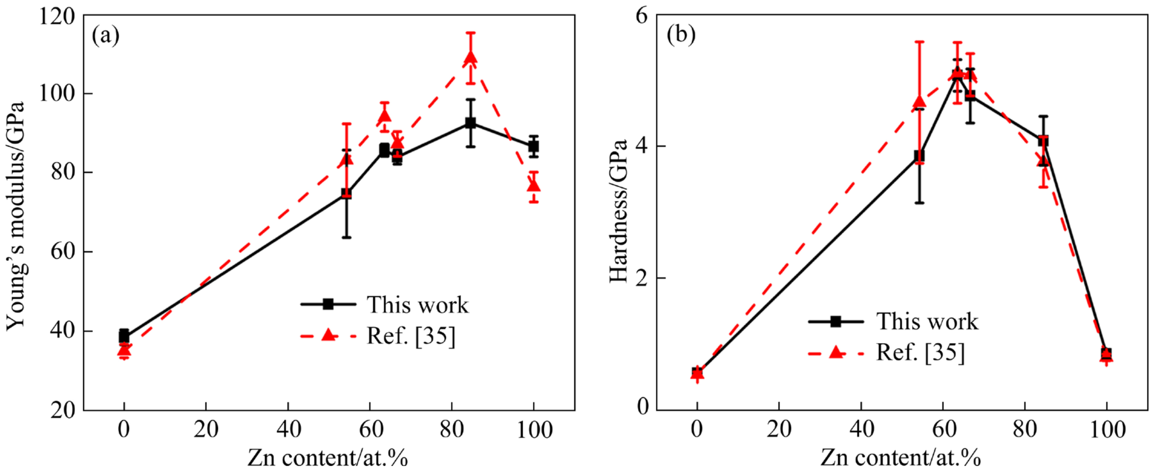

Fig. 4 Variation tendency of Young's modulus (a) and hardness (b) with Zn content for precipitates in Mg−Zn alloys

Table 3 Young's modulus and hardness of precipitates in Mg−Zn alloys and those of pure Mg and Zn

Species	Young's modulus/GPa	Hardness/GPa
Mg	38.48±1.89 (35.02±1.69 [35])	0.56±0.06 (0.54±0.04 [35])
$Mg_{21}Zn_{25}$	74.69±11.05 (83.25±9.15 [35])	3.85±0.71 (4.66±0.92 [35])
Mg_4Zn_7	85.74±1.54 (94.09±3.64 [35])	5.07±0.24 (5.11±0.46 [35])
$MgZn_2$	83.98±1.76 (87.30±3.10 [35])	4.76±0.41 (5.08±0.32 [35])
Mg_2Zn_{11}	92.55±5.95 (108.94±6.39 [35])	4.08±0.37 (3.76±0.38 [35])
Zn	86.63±2.59 (76.42±3.74 [35])	0.85±0.07 (0.80±0.05 [35])

Table 4 Calculated equilibrium lattice parameters, cohesive energy (E_{coh}) and formation enthalpy ($\Delta_r H_m$) of precipitates in Mg−Zn alloys

Species	Lattice parameter/Å			E_{coh}/ (eV·atom^{-1})	$\Delta_r H_m$/ (eV·atom^{-1})
	a	*b*	*c*		
Mg	3.222 (3.19 [36])	3.222 (3.19 [36])	5.171 (5.23 [36])	0	0
$Mg_{21}Zn_{25}$	25.526 (25.64 [36])	25.526 (25.64 [36])	8.674 (8.714 [36])	−1.734	−0.160
Mg_4Zn_7	25.978 (25.96 [31])	5.106 (5.24 [31])	14.398 (14.28 [31])	−1.743	−0.188
$MgZn_2$	5.191 (5.23 [37])	5.191 (5.23 [37])	8.579 (8.56 [37])	−1.740	−0.180
Mg_2Zn_{11}	8.514 (8.462 [35])	8.514 (8.462 [35])	8.514 (8.462 [35])	−1.666	−0.140
Zn	2.750 (2.66 [38])	2.750 (2.66 [38])	4.641 (4.86 [38])	0	0

the compound can be formed and remain stable. Moreover, a smaller formation enthalpy is corresponding to a higher alloying ability of a crystal [40]. Variations of cohesive energy and formation enthalpy with Zn content are shown in Fig. 5. As can be seen, the cohesive energy and formation enthalpy initially decreased and then increased with increasing Zn content. Actually, this is the so-called convex hull. The cohesive energy and formation enthalpy of Mg_4Zn_7 and $MgZn_2$ phases on convex hull are basically the same, indicating that they have the same stability (Fig. 5). These results are in excellent agreement with those obtained by XIE et al [16].

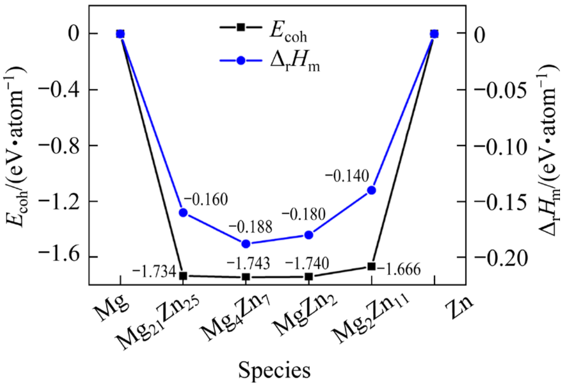

Fig. 5 Variation of cohesive energy and formation enthalpy with Zn content

3.4 Calculated mechanical properties of precipitates

3.4.1 Elasticity

The elastic constant is one of the most important mechanical property parameters and describes the response of a material to applied stress. The elastic constants of the Mg−Zn compounds are calculated based on the stress−strain method and shown in Table 5. There is a fairly good agreement between our calculated results and other available data [16,41−43]. Moreover, these compounds are mechanically stable owing to the elastic constants of these compounds satisfying the Born−Huang stability criteria. The elastic constants along the three principal axes (C_{11}, C_{22} and C_{33}) are different, which shows that these compounds are significantly anisotropic. For Mg, $MgZn_2$ and $Mg_{21}Zn_{25}$, C_{11} is less than C_{33}, indicating that the resistance against deformation along the x-direction is smaller than that along the z-direction, whereas the opposite is true for Mg_2Zn_{11}, Mg_4Zn_7 and Zn (the resistance against deformation along the x-direction is larger than that along the z-direction).

The bulk modulus (B), Young's modulus (E), shear modulus (G) and Poisson's ratio (v) of Mg−Zn alloys are estimated from the elastic constants using Voigt−Reuss−Hill approximation and shown in Table 6. The calculated results agree well with other available values [16,35,41−43]. Moreover, the bulk modulus increased with increasing Zn content, which shows the increased in-compression ability of these compounds. The shear modulus and Young's modulus initially increased and then decreased with increasing Zn content, with the critical point of 63.6 at.% Zn (Mg_4Zn_7). The results reveal that Mg_4Zn_7 has the best shear resistance and stiffness and possesses better comprehensive mechanical properties.

Hardness is one of the important parameters, which reflects the working behaviour of a material, especially for wear-resistant materials. Vickers hardness (H_v) is estimated using the following equation [44]:

$$H_v=2(K^2G)^{0.585}-3,\ K=G/B \tag{5}$$

Table 5 Calculated elastic constants (C_{ij}) of precipitates in Mg−Zn alloys and those of pure Mg and Zn (GPa)

Species	C_{11}	C_{22}	C_{33}	C_{44}	C_{55}	C_{66}	C_{12}	C_{13}	C_{15}	C_{23}	C_{25}	C_{35}	C_{46}
Mg	63.3 (63.5 [41])	–	68.6 (66 [41])	14.8 (19.3 [41])	–	–	33.2 (24.9 [41])	12.7 (20 [41])	–	–	–	–	–
$Mg_{21}Zn_{25}$	87.6	–	111.1	21.9	–	–	39.7	28.3	–	–	–	–	–
Mg_4Zn_7	107.9	139.2	97.6	31.5	25.9	34.3	27.3	32.2	1.4	35.1	0.2	−0.9	0.9
$MgZn_2$	87.3 (92.0 [16])	–	124.4 (126.0 [16])	17.9 (24.0 [16])	–	–	75.1 (62.0 [16])	31.8 (37.0 [16])	–	–	–	–	–
Mg_2Zn_{11}	103.7 (119.2 [42])	–	–	31.4 (32.7 [42])	–	–	45.2 (38.1 [42])	–	–	–	–	–	–
Zn	173.8 (175.5 [43])	–	54.1 (58.7 [43])	38.5 (36.1 [43])	–	–	41.9 (43.2 [43])	46.9 (51.2 [43])	–	–	–	–	–

Table 6 Calculated bulk modulus (B), Young's modulus (E), shear modulus (G), hardness (H_v) and Poisson's ratio (v) of precipitates in Mg−Zn alloys and those of pure Mg and Zn

Species	B_{VRH}/GPa	G_{VRH}/GPa	E/GPa	H_v/GPa	v	G_{VRH}/B_{VRH}
Mg	29.5 (35.8 [41])	12.8 (18.5 [41])	33.5 (47.4 [41])	0.35	0.31 (0.28 [41])	0.43
$Mg_{21}Zn_{25}$	53.2	24.9	66.2	2.39	0.29	0.47
Mg_4Zn_7	54.4 (58.7 [16])	31.2 (31.9 [16])	78.6 (82.1 [16])	4.81	0.26 (0.27 [16])	0.57
$MgZn_2$	57.3 (64.7 [16])	28.4 (22.5 [16])	73.1 (60.5 [16])	3.22	0.39 (0.34 [16])	0.49
Mg_2Zn_{11}	77.6 (67.6 [42])	34.9	88.5	3.27	0.30 (0.27 [42])	0.45
Zn	71.5 (67.8 [43])	26.4 (39.6 [43])	70.5 (76.4 [35])	1.23	0.23	0.37

The calculated results are presented in Table 6, revealing that the hardness initially increased and then decreased with increasing Zn content, which is consistent with the experimental results. The results once again prove the reliability of the calculation and rationality of parameter selection. Moreover, the theoretical hardness and Young's modulus of the Mg−Zn binary compounds are smaller than those of the experimental results. As known, the factors that affect the mechanical properties of a material are not only intrinsic characteristics (atomic bonding) but also an extrinsic characteristic (measuring parameters) [45]. For theoretical calculation, it only considers the influence of atomic bonding when calculating the moduli. The lattice constants obtained by the experiment are usually smaller than the theoretical results, which is conducive to the improvement of moduli and hardness. Thus, the measured Young's modulus and hardness are higher than the theoretical results.

Poisson's ratio (v) can not only reflect the degree of directionality of chemical bonds but also be used to evaluate the ductility or brittleness of a material [26]. From Table 6, Poisson's ratios of the compounds are 0.23−0.39, indicating that they have a combination of metallic, covalent and ionic bonding. Generally, a Poisson's ratio of higher than 0.26 indicates that the compound is ductile. Poisson's ratio initially increased and then decreased with increasing Zn content. Thus, this shows that there is brittle-to-ductile transition. The brittleness or ductility of a material has a great influence on its application in practical engineering. G/B and Cauchy pressures ($C_{12}-C_{44}$) are commonly applied to estimating the ductility or brittleness of a material. If a material has G/B of less than 0.5 and positive $C_{12}-C_{44}$, it is ductile and vice versa [25]. Figure 6 shows the ductility diagram of the Mg−Zn compounds. It is shown that $MgZn_2$, Mg_2Zn_{11} and $Mg_{21}Zn_{25}$ are clearly ductile while Mg_4Zn_7 is brittle. The decreasing order of ductility for these compounds is $MgZn_2 > Mg_{21}Zn_{25} > Mg_2Zn_{11} > Mg_4Zn_7$. The results reveal that ductility initially increased and then decreased with increasing Zn content. Additionally, the results from the change in G/B are in excellent agreement with the results from Poisson's ratio. From the analysis of the above results, it can be concluded that the addition of an appropriate amount of Zn (for example, 67 at.%) is expected to simultaneously improve the strength and plasticity of Mg alloys.

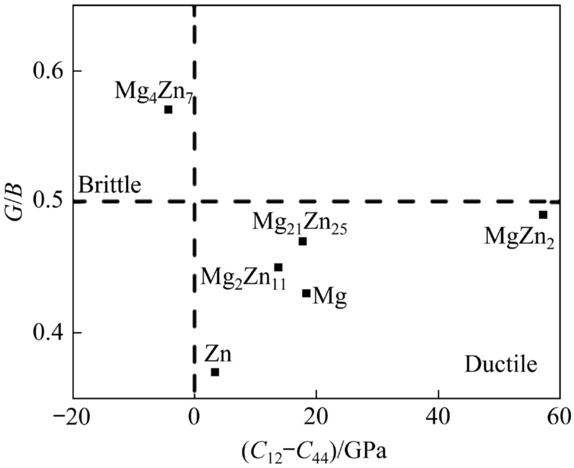

Fig. 6 Ductility diagram of precipitates in Mg−Zn alloys

3.4.2 Elastic anisotropy

The elastic anisotropy of a crystal not only shows different bonding properties in different directions but also is related to the possibility of microcracks in a material, which has important significance. In this study, the universal factor (A^U) and elastic anisotropy indexes (A_B, A_G) are calculated to measure the elastic anisotropy possessed by a crystal using the following equations:

$$A^{\mathrm{U}}=5\frac{G_{\mathrm{V}}}{G_{\mathrm{R}}}+\frac{B_{\mathrm{V}}}{B_{\mathrm{R}}}-6\geq 0 \tag{6}$$

$$A_{\mathrm{B}}=\frac{B_{\mathrm{V}}-B_{\mathrm{R}}}{B_{\mathrm{V}}+B_{\mathrm{R}}} \tag{7}$$

$$A_{\mathrm{G}}=\frac{G_{\mathrm{V}}-G_{\mathrm{R}}}{G_{\mathrm{V}}+G_{\mathrm{R}}} \tag{8}$$

Table 7 shows the universal factor and elastic anisotropy indexes of these compounds. The universal factor is an important parameter to characterize the anisotropy of a material. It is known that a larger universal factor means that the material is more anisotropic and a universal factor equal to zero means that it is isotropic. From Table 7, it can be found that these compounds have obvious anisotropic characteristics. The decreasing order of anisotropy is $MgZn_2 > Mg_4Zn_7 > Mg_{21}Zn_{25} > Mg_2Zn_{11}$. The results reveal that the strength of anisotropy initially increased and then decreased with increasing Zn content.

In addition to these anisotropy factors, the anisotropy behaviour can be better understood by describing the three-dimensional (3D) surface construction of Young's modulus. Different crystalline systems have different surface contour calculation formulas. The specific method can refer to previous work [25,46]. Figure 7 gives the 3D surface contours of Young's modulus for these compounds. From Fig. 7, it can be seen that the surface morphology of the compounds is clearly different from the spheres. The results reveal that these compounds exhibit significant anisotropy,

Table 7 Calculated universal factor (A^{U}) and elastic anisotropy indexes (A_{B}, A_{G}) of precipitated phases in Mg−Zn alloys and those of pure Mg and Zn

Species	A^{U}	A_{B}	A_{G}
Mg	2.733	0.001	0.215
$Mg_{21}Zn_{25}$	0.266	0.001	0.026
Mg_4Zn_7	2.137	0.176	0.146
$MgZn_2$	4.393	0.001	0.305
Mg_2Zn_{11}	0.004	0	0.001
Zn	1.925	0.148	0.141

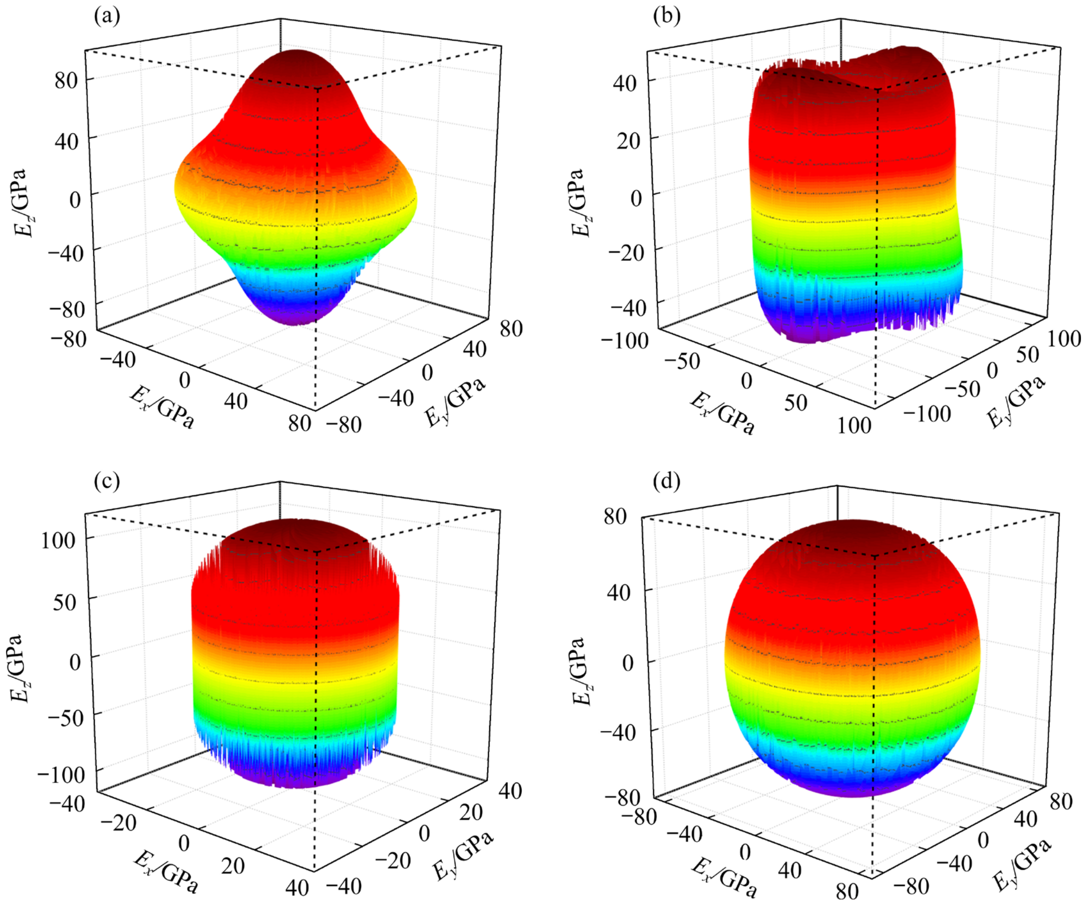

Fig. 7 3D surface contours of Young's modulus for precipitates in Mg−Zn alloys: (a) $Mg_{21}Zn_{25}$; (b) Mg_4Zn_7; (c) $MgZn_2$; (d) Mg_2Zn_{11}

which are essentially consistent with the calculated anisotropy factors. In other words, the mechanical anisotropy of the compounds initially increased and then decreased with increasing Zn content. As known, mechanical anisotropy is usually derived from directional covalent bonds. Therefore, it shows that there is a strong covalent bonding character in these compounds, especially in $MgZn_2$. To explain the anisotropy properties of Young's modulus more directly, planar projections on the (100) and (110) planes are constructed, as shown in Fig. 8. It is revealed that $MgZn_2$ and Mg_4Zn_7 show more anisotropy than the other compounds because they are distinct from the sphere. The results once again prove the reliability of the universal factor (A^U). The Young's modulus of the compound is different in different directions, indicating that Young's modulus changes with the direction. $MgZn_2$ has the largest Young's modulus along the [001] direction, and Mg_4Zn_7 has the largest Young's modulus along the [010] direction on the (100) plane. Moreover, Young's modulus along the [110] direction decreases initially and then increases with increasing Zn content. Mg_2Zn_{11} has the largest Young's modulus along the [111] direction.

3.5 Electronic properties

To clarify the influence of Zn content on the chemical bonding properties of the compound, the total density of states (TDOS) and partial density of states (PDOS) of Mg−Zn compounds are estimated (Fig. 9). The black dashed line means the Fermi energy level. These compounds display obvious metallic characteristics because the TDOS at the Fermi level are non-zero. From Fig. 9, it can be found that the TDOS values at Fermi level are 82.69, 29.11, 4.75 and 10.82 state/eV for $Mg_{21}Zn_{25}$, Mg_4Zn_7, $MgZn_2$ and Mg_2Zn_{11}, respectively. This reveals that $MgZn_2$ is the most stable compound in the Mg−Zn compounds, which coincides with the analysis of the formation enthalpy. Moreover, it is important to note that these compounds appear to have a deep valley near the Fermi level, which is called a pseudo-gap. It is usually utilized to characterize the presence of a strongly directed covalent bonding, indicating a stronger covalent bonding. It can be obtained from the TDOS that Mg_4Zn_7 has a stronger covalent bonding. However, strongly directed covalent bonding causes a heterogeneous distribution [47,48], indicating that Mg_4Zn_7 is a brittle fracture along the direction of weak bonding. Moreover, from the PDOS analysis, the TDOS peak is dominated by the Zn-d states in the valence band, whereas it is determined using the Mg-p, Mg-s and Zn-p states in the conduction band. Near the Fermi level, the Mg-p and Zn-d states are overlapped, which shows that the p−d hybridization between the Mg and Zn atoms forms strong covalent bonding. Thus, it is concluded that the chemical bonding of these compounds consists of metallic and covalent bonds.

To further characterize and quantify the strength of the covalent bond, population analysis and bond length are analyzed. In this study, the Mulliken method is utilized to evaluate the average bond population ($\overline{n}$) and mean bond length ($\overline{L}$), to illustrate the effect of Zn content on the chemical bonds of the Mg−Zn compounds. The corresponding

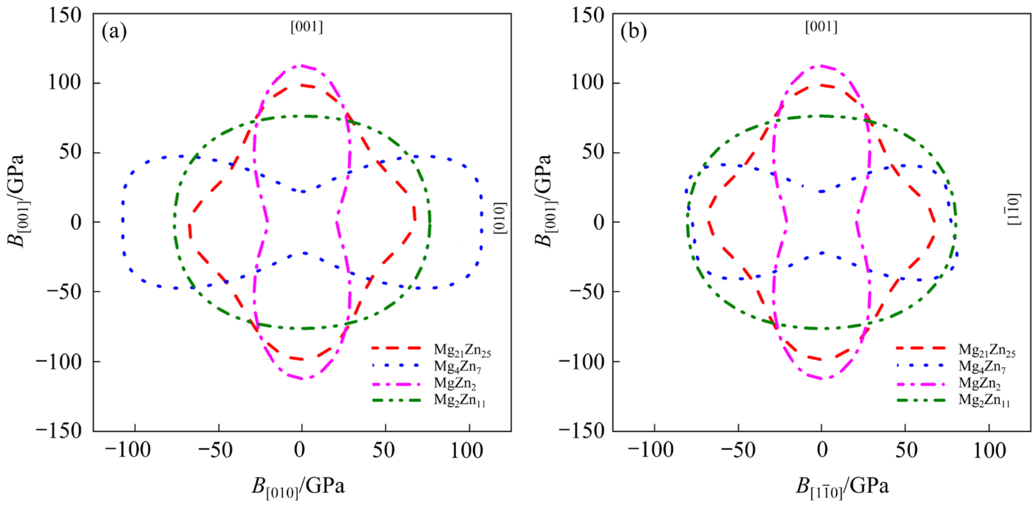

Fig. 8 Planar projections of Young's modulus for precipitates in Mg−Zn alloys on different crystallographic planes: (a) (100) plane; (b) (110) plane

expressions are as follows:

$$\bar{n}=\sum_{i=1}^{N}(n_iN_i)\Big/\sum_{i=1}^{N}N_i \tag{9}$$

$$\bar{L}=\sum_{i=1}^{N}(L_iN_i)\Big/\sum_{i=1}^{N}N_i \tag{10}$$

where n_i, N_i and L_i respectively refer to the bond population, total bond number and bond length of the i bond in the cell. Table 8 lists the calculated average bond populations and mean bond lengths. It can be seen that Mg atoms have a positive charge and Zn atoms carry a negative charge. The results mean that electrons can be transferred from Mg to Zn atoms, resulting in hybridization between the Mg and Zn atoms and the formation of covalent bonding. The charges of Mg and Zn atoms increase

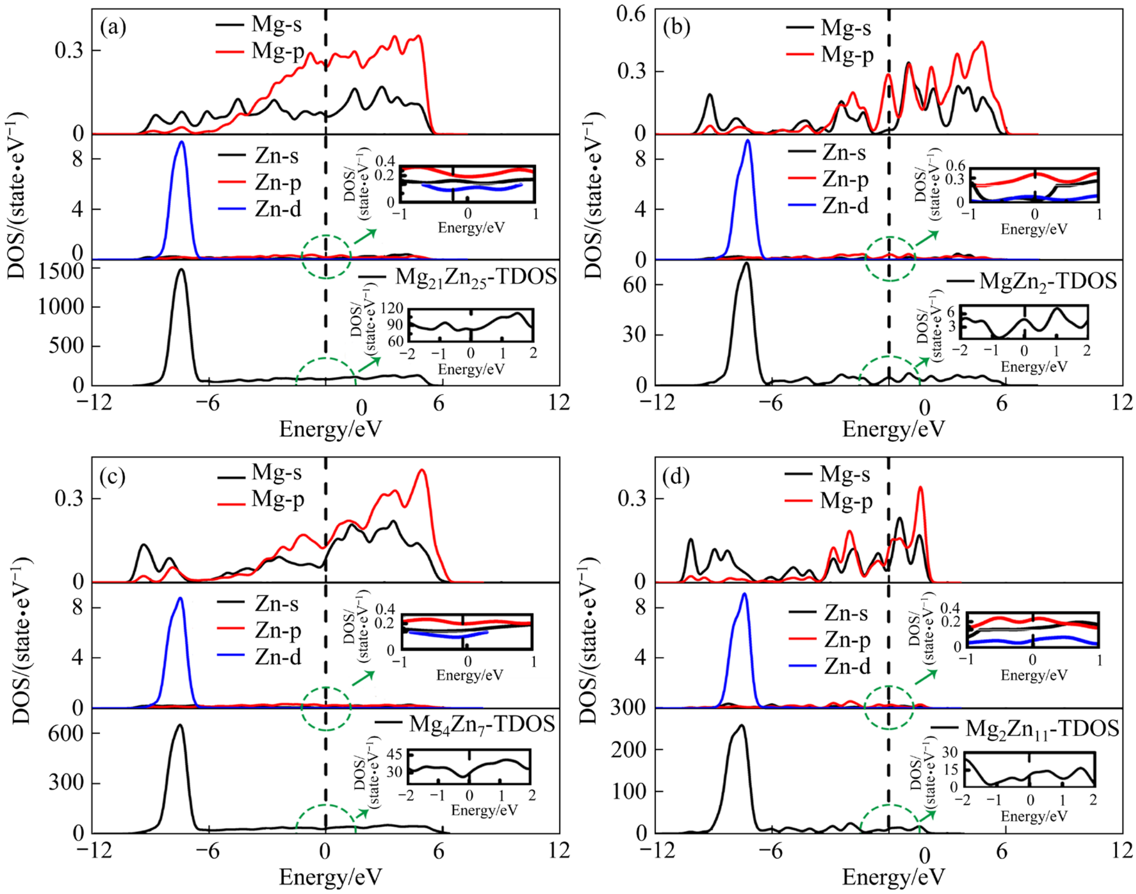

Fig. 9 TDOS and PTOS for precipitates in Mg−Zn alloys: (a) $Mg_{21}Zn_{25}$; (b) $MgZn_2$; (c) Mg_4Zn_7; (d) Mg_2Zn_{11}

Table 8 Calculated average bond length ($\bar{L}$) and mean bond population ($\bar{n}$) of precipitates in Mg−Zn alloys

Species	Atom	Charge/e	Bond	$\bar{n}$	$\bar{L}$/Å
$Mg_{21}Zn_{25}$	Mg	0.728	Mg—Zn	0.11	2.949
	Zn	−0.612	Zn—Zn	0.52	2.636
			Mg—Mg	0.05	2.973
Mg_4Zn_7	Mg	0.925	Mg—Zn	0.04	2.922
	Zn	−0.528	Zn—Zn	0.51	2.628
			Mg—Mg	0.04	2.994
$MgZn_2$	Mg	1.030	Zn—Zn	0.40	2.605
	Zn	−0.513			
Mg_2Zn_{11}	Mg	1.230	Mg—Zn	0.01	2.941
	Zn	−0.223	Zn—Zn	0.61	2.668

with increasing Zn content. Moreover, the bonding exhibits metallic characteristics, mainly because the bond population is arranged in positive mode. The bond length of Mg—Zn bonding is larger than that of Zn—Zn bonding, indicating weak Mg—Zn bonding. The bond population and bond length of Zn—Zn bonding in the Mg−Zn compounds initially decreased and then increased with increasing Zn content. The results reveal that both the covalency degree of bonding and bond length of covalent bonds initially increased and then decreased with increasing Zn content, which coincides with the mechanical properties analysis.

4 Conclusions

(1) The main precipitates ($Mg_{21}Zn_{25}$, Mg_4Zn_7, $MgZn_2$ and Mg_2Zn_{11}) in the Mg−Zn alloys were investigated. The nano-indentation results reveal that the hardness of the precipitates initially increased and then decreased with increasing Zn content and the hardness of all precipitates was significantly higher than that of pure Mg and Zn.

(2) The phase stability initially increased and then decreased with increasing Zn content. The bulk moduli of these compounds increased, whereas their shear and Young's moduli initially increased and then decreased with increasing Zn content. The calculated hardness of these compounds initially increased and then decreased with an increase in Zn content, which are consistent with the experimental results. The decreasing order of ductility for these compounds is $MgZn_2 > Mg_{21}Zn_{25} > Mg_2Zn_{11} > Mg_4Zn_7$. The mechanical anisotropy initially increased and then decreased with increasing Zn content.

(3) The chemical bonding of these compounds consists of metallic and covalent bonds. Both the covalency degree of bonding and bond length of covalent bonds initially increased and then decreased with increasing Zn content, which coincides with the mechanical properties analysis.

CRediT authorship contribution statement

Tian-zhi ZHANG: Methodology, Software, Data curation, Writing − Original draft; **Yang-zhen LIU:** Conceptualization, Writing − Review & editing; **Qing-yun FU:** Visualization, Investigation; **Bai-song GUO:** Data curation, Validation; **Wei-hong JIN:** Resources, Formal analysis; **Zhen-tao YU:** Supervision, Conceptualization, Writing − Review & editing.

Declaration of competing interest

The authors declare that they have no known competing financial interests or personal relationships that could have appeared to influence the work reported in this paper.

Acknowledgments

The authors would like to thank the financial support from Guangdong Basic and Applied Basic Research Foundation, China (Nos. 2020B1515120078, 2020A1515111067, 2021A1515010890).

References

[1] LIAO H B, MO L L, LI C B, ZHAN M Y, DU J. Grain refinement of Mg−Al binary alloys inoculated by in-situ oxidation [J]. Transactions of Nonferrous Metals Society of China, 2022, 32(10): 3212−3221.

[2] LIU W, WU B Q, LIU H R, LIU R S, MO Y F, TIAN Z A, HOU Z Y, XI T F, WAN Z Y, HUANG C X, CHEN X. Simulation on microstructure evolution and mechanical properties of Mg−Y alloys: Effect of trace Y [J]. Transactions of Nonferrous Metals Society of China, 2022, 32(3): 812−823.

[3] ZHANG K L, LI H Z, LIANG X P, CHEN Z, ZHAO Z X, TAO H, ZHOU X W. Effect of aging time on discontinuous precipitates, continuous precipitates and mechanical properties of AZ80A magnesium alloy [J]. Transactions of Nonferrous Metals Society of China, 2022, 32(9): 2838−2851.

[4] WANG C, YANG H I, LI X, ZHENG Y F. In vitro evaluation of the feasibility of commercial Zn alloys as biodegradable metals [J]. Journal of Materials Science & Technology, 2016, 32(9): 909−918.

[5] ZHANG E L, YANG L, XU J W, CHEN H Y. Microstructure, mechanical properties and bio-corrosion properties of Mg−Si (−Ca, Zn) alloy for biomedical application [J]. Acta Biomaterialia, 2010, 6(5): 1756−1762.

[6] HEIMANN R B. Magnesium alloys for biomedical application: Advanced corrosion control through surface coating [J]. Surface and Coatings Technology, 2021, 405: 126521.

[7] TAYLOR S, WEST G D, MOGIRE E, TANG F, KOTADIA H R. Superplastic forming characteristics of AZ41 magnesium alloy [J]. Transactions of Nonferrous Metals Society of China, 2021, 31(3): 648−654.

[8] DING Y, WEN C, HODGSON P, LI Y. Effects of alloying elements on the corrosion behavior and biocompatibility of biodegradable magnesium alloys: A review [J]. Journal of Materials Chemistry B, 2014, 2(14): 1912−1933.

[9] HOU C H, YE Z S, QI F G, WANG Q, LI L H, OUYANG X P, ZHAO N. Effect of Al addition on microstructure and mechanical properties of Mg−Zn−Sn−Mn alloy [J]. Transactions of Nonferrous Metals Society of China, 2021, 31(7): 1951−1968.

[10] DONG Q, LUO Z, ZHU H, WANG L, YING T, JIN Z, LI D, DING W, ZENG X. Basal-plane stacking-fault energies of Mg alloys: A first-principles study of metallic alloying effects [J]. Journal of Materials Science & Technology, 2018, 34(10): 1773−1780.

[11] TIAN Z, YANG Q, GUAN K, CAO Z Y, MENG J. Microstructural evolution and aging behavior of Mg−4.5Y−2.5Nd−1.0Gd−0.5Zr alloys with different Zn additions [J]. Rare Metals, 2021, 40(8): 2188−2196.

[12] JANBOZORGI M, TAHERI K K, TAHERI A K. Microstructural evolution, mechanical properties, and corrosion resistance of a heat-treated Mg alloy for the bio-medical application [J]. Journal of Magnesium and Alloys, 2019, 7(1): 80−89.

[13] PAN H, PANG K, CUI F, GE F, MAN C, WANG X, CUI Z. Effect of alloyed Sr on the microstructure and corrosion behavior of biodegradable Mg−Zn−Mn alloy in Hanks' solution [J]. Corrosion Science, 2019, 157: 420−437.

[14] El-MAHALLAWY N, PALKOWSKI H, KLINGNER A, DIAA A, SHOEIB M. Effect of 1.0 wt.% Zn addition on the microstructure, mechanical properties, and bio-corrosion behaviour of micro alloyed Mg−0.24Sn−0.04Mn alloy as biodegradable material [J]. Materials Today Communications, 2020, 24: 100999.

[15] LIU S, ESTEBAN-MANZANARES G, LLORCA J. First-principles analysis of precipitation in Mg−Zn alloys [J]. Physical Review Materials, 2020, 4(9): 093609.

[16] XIE Y P, WANG Z Y, HOU Z. The phase stability and elastic properties of $MgZn_2$ and Mg_4Zn_7 in Mg−Zn alloys [J]. Scripta Materialia, 2013, 68(7): 495−498.

[17] WANG D, AMSLER M, HEGDE V I, SAAL J E, ISSA A, ZHOU B C, ZENG X, WOLVERTON C. Crystal structure, energetics, and phase stability of strengthening precipitates in Mg alloys: A first-principles study [J]. Acta Materialia, 2018, 158: 65−78.

[18] KIM K, ROY A, GURURAJAN M, WOLVERTON C, VOORHEES P. First-principles/phase-field modeling of θ' precipitation in Al−Cu alloys [J]. Acta Materialia, 2017, 140: 344−354.

[19] KIM K, ZHOU B C, WOLVERTON C. First-principles study of crystal structure and stability of $T1$ precipitates in Al−Li−Cu alloys [J]. Acta Materialia, 2018, 145: 337−346.

[20] MAO Z, CHEN W, SEIDMAN D N, WOLVERTON C. First-principles study of the nucleation and stability of ordered precipitates in ternary Al−Sc−Li alloys [J]. Acta Materialia, 2011, 59(8): 3012−3023.

[21] OUYANG Y, CHEN H, TAO X, GAO F, PENG Q, DU Y. A first-principles study of the structural, mechanical and electronic properties of precipitates of Al_2Cu in Al−Cu alloys [J]. Physical Chemistry Chemical Physics, 2018, 20(2): 967−976.

[22] SEGALL M, LINDAN P J, PROBERT M A, PICKARD C J, HASNIP P J, CLARK S, PAYNE M. First-principles simulation: Ideas, illustrations and the CASTEP code [J]. Journal of Physics: Condensed Matter, 2002, 14(11): 2717−2744.

[23] PERDEW J P, BURKE K, ERNZERHOF M. Generalized gradient approximation made simple [J]. Physical Review Letters, 1996, 77(18): 3865−3868.

[24] LIU T, CHONG X Y, YU W, ZHOU Y X, HUANG H G, ZHOU R F, FENG J. Changes of alloying elements on elasticity and solid solution strengthening of α-Ti alloys: A comprehensive high-throughput first-principles calculations [J]. Rare Metals, 2022, 41(8): 2719−2731.

[25] LIU Y, ZHANG L, CUI S, LI W. Effects of transition metal (Cr, Mn, Mo, Ni, Ti, and V) doping on the mechanical, electronic and thermal properties of Fe_3Al [J]. Vacuum, 2021, 185: 110030.

[26] XIAO P, GAO Y, YANG C, DONG Y, HUANG X, WANG Y, YANG S. Effect of Sb doping on microstructure, mechanical and electronic properties of Mg_2Si in Mg_2Si/AZ91 composites by experimental investigation and first-principles calculation [J]. Journal of Alloys and Compounds, 2022, 902: 163859.

[27] LIU Y, ZHENG B, JIAN Y, ZHANG L, YI Y, LI W. Anisotropic in elasticity, sound velocity and minimum thermal conductivity of Al−Cu intermetallic compounds [J]. Intermetallics, 2020, 124: 106880.

[28] WU Z J, ZHAO E J, XIANG H P, HAO X F, LIU X J, MENG J. Crystal structures and elastic properties of superhard IrN_2 and IrN_3 from first principles [J]. Physical Review B, 2007, 76(5): 054115.

[29] YAO C, WANG Z, TAY S L, ZHU T, GAO W. Effects of Mg on microstructure and corrosion properties of Zn−Mg alloy [J]. Journal of Alloys and Compounds, 2014, 602: 101−107.

[30] de NEGRI S, SKROBANSKA M, DELFINO S, SACCONE A. The Mg−Zn−Si system: Constitutional properties and phase formation during mechanical alloying [J]. Intermetallics, 2010, 18(9): 1722−1728.

[31] YAN K, BAI J, LIU H, JIN Z Y. The precipitation behavior of $MgZn_2$ and Mg_4Zn_7 phase in Mg−6Zn (wt.%) alloy during equal-channel angular pressing [J]. Journal of Magnesium and Alloys, 2017, 5(3): 336−339.

[32] CAI S, LEI T, LI N, FENG F. Effects of Zn on microstructure, mechanical properties and corrosion behavior of Mg−Zn alloys [J]. Materials Science and Engineering C, 2012, 32(8): 2570−2577.

[33] OLIVER W C, PHARR G M. Nanoindentation in materials research: Past, present, and future [J]. MRS Bulletin, 2010, 35(11): 897−907.

[34] OLIVER W C, PHARR G M. Measurement of hardness and elastic modulus by instrumented indentation: Advances in understanding and refinements to methodology [J]. Journal of Materials Research, 2004, 19(1): 3−20.

[35] KAMMERER C, BEHDAD S, ZHOU L, BETANCOR F, GONZALEZ M, BOESL B, SOHN Y. Diffusion kinetics, mechanical properties, and crystallographic characterization of intermetallic compounds in the Mg−Zn binary system [J]. Intermetallics, 2015, 67: 145−155.

[36] ZHOU L, SU K, WANG Y, ZENG Q, LI Y. First-principles study of the properties of Li, Al and Cd doped Mg alloys [J]. Journal of Alloys and Compounds, 2014, 596: 63−68.

[37] MAO P, YU B, LIU Z, WANG F, JU Y. First-principles calculations of structural, elastic and electronic properties of AB_2 type intermetallics in Mg−Zn−Ca−Cu alloy [J]. Journal of Magnesium and Alloys, 2013, 1(3): 256−262.

[38] NITOL M S, DICKEL D E, BARRETT C D. Artificial

neural network potential for pure zinc [J]. Computational Materials Science, 2021, 188: 110207.

[39] ZHANG J, MAO C, LONG C, CHEN J, TANG K, ZHANG M, PENG P. Phase stability, elastic properties and electronic structures of Mg−Y intermetallics from first-principles calculations [J]. Journal of Magnesium and Alloys, 2015, 3(2): 127−133.

[40] ZARKEVICH N A, TAN T L, JOHNSON D D. First-principles prediction of phase-segregating alloy phase diagrams and a rapid design estimate of their transition temperatures [J]. Physical Review B, 2007, 75(10): 104203.

[41] GANESHAN S, SHANG S, WANG Y, LIU Z K. Effect of alloying elements on the elastic properties of Mg from first-principles calculations [J]. Acta Materialia, 2009, 57(13): 3876−3884.

[42] LIU X L, VANLEEUWEN B K, SHANG S L, DU Y, LIU Z K. On the scaling factor in Debye–Grüneisen model: A case study of the Mg−Zn binary system [J]. Computational Materials Science, 2015, 98: 34−41.

[43] IWAOKA H, HIROSAWA S. First-principles calculation of elastic properties of Cu−Zn intermetallic compounds for improving the stiffness of aluminum alloys [J]. Computational Materials Science, 2020, 174: 109479.

[44] WEI Z Y, HU K M, SA B S, WU B. Pressure-induced structure, electronic, thermodynamic and mechanical properties of Ti_2AlNb orthorhombic phase by first-principles calculations [J]. Rare Metals, 2021, 40(10): 1−11.

[45] FARHADIZADEH A R, AMADEH A A, GHOMI H. The effect of metal transition dopant on electronic and mechanical properties of titanium nitride: First principle method [J]. Computational Materials Science, 2018, 141: 82−90.

[46] JIAN Y, HUANG Z, XING J, SUN L, LIU Y, GAO P. Phase stability, mechanical properties and electronic structures of TiAl binary compounds by first principles calculations [J]. Materials Chemistry and Physics, 2019, 221: 311−321.

[47] HU H, WU X, WANG R, LI W, LIU Q. Phase stability, mechanical properties and electronic structure of TiAl alloying with W, Mo, Sc and Yb: First-principles study [J]. Journal of Alloys and Compounds, 2016, 658: 689−696.

[48] HU H, WU X, WANG R, JIA Z, LI W, LIU Q. Structural stability, mechanical properties and stacking fault energies of $TiAl_3$ alloyed with Zn, Cu, Ag: First-principles study [J]. Journal of Alloys and Compounds, 2016, 666: 185−196.

Mg−Zn 合金析出相的结构、力学和电子特性

张添植[1]，刘洋赈[1,2]，符青云[3]，郭柏松[1]，金卫红[1]，于振涛[1]

1. 暨南大学 先进耐磨蚀及功能材料研究院，广州 510632；
2. 暨南大学 韶关研究院，韶关 512027；
3. 南方医科大学 口腔医院，广州 510280

摘　要：为了加快镁(Mg)合金的开发和设计，通过实验和密度泛函理论研究 Mg−Zn 合金中重要析出相的结构和力学性能。纳米压痕试验显示，析出相硬度随锌含量的增加先增加后降低，且明显高于纯镁和锌的硬度。计算结果显示，析出相的稳定性随着锌含量的增加先增加后降低。析出相的体积模量随着锌含量的增加而增大，而其剪切模量和杨氏模量随着锌含量的增加先增大后减小。这些化合物延展性由高到低的顺序为 $MgZn_2 > Mg_{21}Zn_{25} > Mg_2Zn_{11} > Mg_4Zn_7$。这些化合物的表面轮廓表明其具有明显的各向异性。共价键的共价程度和键长随锌含量的增加先增大后减小。

关键词：镁锌合金；纳米压痕；模量；硬度；化学键

(Edited by Wei-ping CHEN)